Int. J. Electrochem. Sci., 16 **(2021)** Article ID: 210933, doi: 10.20964/2021.09.45

International Journal of
ELECTROCHEMICAL
SCIENCE
www.electrochemsci.org

Effect of Ti-doping and Octahedral Morphology on Electrochemical Performance of Lithium Manganate Oxide as Cathode Materials for LIBs

Yongfeng Li[1], *Gan Zhu*[1], *Qiwen Ran*[2,*], *Jintao Liu*[2], *Yu Zhou*[1], *Mengyuan Zhao*[1], *Peng Cao*[2], *Hongyuan Zhao*[1,*]

[1] Research Center for Advanced Materials and Electrochemical Technology, Henan Institute of Science and Technology, Xinxiang, 453003, China
[2] School of Materials and Energy, University of Electronic Science and Technology of China, Chengdu 610054, China
[3] Department of Chemical and Materials Engineering, The University of Auckland, Private Bag 92019, Auckland, 1142, New Zealand
[*]E-mail: qiwenran@yeah.net (Q. Ran), hongyuanzhao@126.com (H. Zhao)

Received: 2 June 2021 / *Accepted:* 20 July 2021 / *Published:* 10 August 2021

This work proposed a collaborative strategy of Ti-doping and octahedral morphology to improve the cycling property of lithium manganate oxide ($LiMn_2O_4$). The $LiTi_{0.05}Mn_{1.95}O_4$ octahedrons were prepared by solid-phase method with Mn_3O_4 octahedrons and TiO_2 nanoparticles as manganese precursor and titanium dopant, respectively. XRD and SEM characterizations indicated that the existence of tetravalent titanium ions presents no substantive impact on the spinel structure. The obtained $LiTi_{0.05}Mn_{1.95}O_4$ sample well inherited the octahedral morphology of Mn_3O_4 octahedrons. For this sample, the Ti-doping could enhance the crystal structure stability and avoid the reduction of trivalent manganese ions, and the octahedral morphology helped to maintain the spinel structure by inhibiting the manganese dissolution. These functions could effectively enhance the cycling stability of $LiMn_2O_4$. When tested at 1.0 C, the 1st reversible capacity of $LiTi_{0.05}Mn_{1.95}O_4$ octahedrons was higher than that of both the $LiTi_{0.05}Mn_{1.95}O_4$ particles and $LiMn_2O_4$ particles. After 100 cycles, the capacity retention of $LiTi_{0.05}Mn_{1.95}O_4$ octahedrons could reach up to 94.2%, which was much higher than that of other two samples (90.3% and 75.2%). Furthermore, the high-rate capability and high-temperature performance were significantly improved due to the synergetic modification of Ti-doping and octahedral morphology.

Keywords: Lithium manganate; Titanium doping; Octahedral morphology; Cycling stability; Synergistic effect

1. INTRODUCTION

Cathode materials have an important impact on the manufacturing cost and charge-discharge property of lithium-ion batteries [1-3]. Lithium manganate oxide ($LiMn_2O_4$) has many advantages such

as rich manganese resources, cheap production cost, mature manufacturing technology, which are conducive to the practical application of $LiMn_2O_4$ [4-7]. However, it is somewhat regrettable that the poor cycling stability of this cathode material has a serious negative impact on the long battery life. According to the reported works, the poor cycling stability has strong connections with Jahn-Teller distortion, surface Mn dissolution, and particle aggregation, which severely disrupt the structural stability of $LiMn_2O_4$ [8-11].

To inhibit the Jahn-Teller distortion, a great many of scientific researchers modified the structural stability of $LiMn_2O_4$ by introducing some heterogeneous ions to replace the manganese ions. The corresponding ions mainly involve negative nonmetal ions (F^-, Cl^-) [12, 13], low-value metal ions (Li^+, Cu^{2+}, Mg^{2+}, Al^{3+}, Er^{3+}) [5, 14-17], high-value nonmetal/metal ions (Sn^{4+}, Si^{4+}, Ti^{4+}, V^{5+}) [18-22]. Among these ions, high-value nonmetal/metal ions can show extra effect of avoiding the reduction of trivalent manganese ions, which have much to do with the reversible specific capacity. Several research works confirmed that the Ti-doping could enhance the crystal structure stability because of the stronger Ti-O chemical bond and inhibited Jahn-Teller distortion in the crystal structure but also avoid the reduction of trivalent manganese ions [20, 23]. Xiong [20] synthesized the tetravalent titanium-doped lithium manganate oxide by high-temperature solid state method. The results showed that the introduction of tetravalent titanium ions could enhance the strength of chemical bonds and reduce the degeneracy of manganese ions, which improved the structure stability. Xue [24] prepared the titanium doped lithium manganese oxide nanorods, which confirmed the positive function of Ti-doping on the reversible specific capacity. These research results indicated that the Ti-doping is a valuable strategy to improve the electrochemical performance of $LiMn_2O_4$. Furthermore, several reported works demonstrated that the octahedral morphology helped to realize the improvement of cycling stability by inhibiting the manganese dissolution to maintain the structure stability of $LiMn_2O_4$ [25, 26]. Jin [26] successfully synthesized the $LiMn_2O_4$ octahedrons with the hydrothermally synthesized Mn_3O_4 octahedrons as manganese precursor, which effectively achieved the improvement of capacity retention.

Herein, the $LiTi_{0.05}Mn_{1.95}O_4$ octahedrons was prepared through a solid-phase process with Mn_3O_4 octahedrons as manganese precursor and TiO_2 nanoparticles as titanium dopant. The Ti-doping could enhance the crystal structure stability and avoid the reduction of trivalent manganese ions, and the octahedral morphology helped to maintain the spinel structure by inhibiting the manganese dissolution. Compared with the existing research works, the synergistic effect of Ti-doping and octahedral morphology significantly enhanced the electrochemical properties of $LiMn_2O_4$, which has important value and significance in the development of this cathode material.

2. EXPERIMENTAL

2.1. Materials synthesis

The $LiTi_{0.05}Mn_{1.95}O_4$ octahedrons was prepared through a solid-phase lithium intercalation process. The manganese precursor Mn_3O_4 octahedrons was first synthesized by a simple and low-cost hydrothermal reaction process. Subsequently, a certain amount of Mn_3O_4 octahedrons, TiO_2 nanoparticles, and $LiOH \cdot H_2O$ were mixed by means of ethanol. The corresponding grinding-mixing

process was repeated for three times. The obtained mixture was dried in vacuum and further headed at 800 °C for 10 h in air atmosphere. For comparison, both the $LiTi_{0.05}Mn_{1.95}O_4$ and $LiMn_2O_4$ samples with irregular morphology were synthesized with electrolytic MnO_2 (EMD) and $LiOH·H_2O$ as raw materials. In the following description, these two samples with irregular morphology were marked as $LiTi_{0.05}Mn_{1.95}O_4$ particles and $LiMn_2O_4$ particles, respectively.

The obtained $LiTi_{0.05}Mn_{1.95}O_4$ octahedrons, $LiTi_{0.05}Mn_{1.95}O_4$ particles, and $LiMn_2O_4$ particles were characterized based on the analytical techniques such as XRD and SEM. XRD pattern was applied to analyze the effect of Ti-doping on the phase structure of $LiMn_2O_4$, and SEM image was used to confirm the effect of Ti-doping on the surface morphology of $LiMn_2O_4$. The influence of Ti-doping and octahedral morphology on the electrochemical properties of $LiMn_2O_4$ was investigate thoroughly by means of LANHE CT2001A battery tester and CHI660E electrochemical workstation.

3. RESULTS AND DISCUSSION

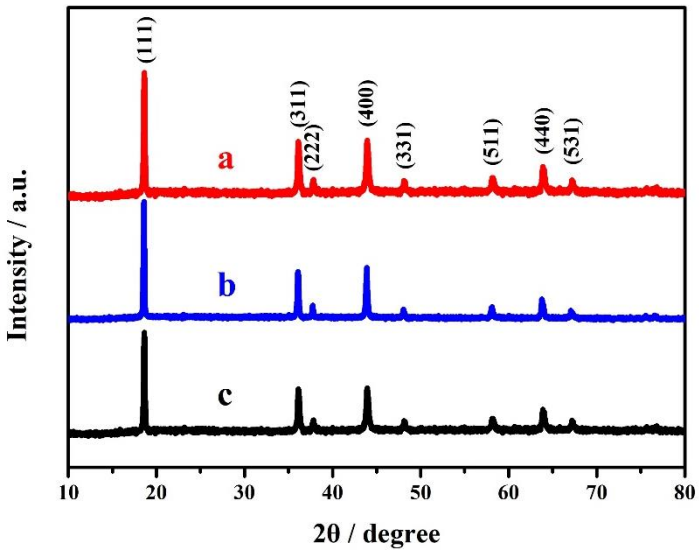

Figure 1. XRD patterns of (a) $LiTi_{0.05}Mn_{1.95}O_4$ octahedrons, (b) $LiTi_{0.05}Mn_{1.95}O_4$ particles, and (c) $LiMn_2O_4$ particles.

Fig. 1 provides the XRD patterns of the obtained $LiTi_{0.05}Mn_{1.95}O_4$ octahedrons, $LiTi_{0.05}Mn_{1.95}O_4$ particles, and $LiMn_2O_4$ particles. All the diffraction peaks of $LiMn_2O_4$ particles completely correspond to the characteristic peaks of $LiMn_2O_4$ (JCPDS No. 35-0782) [7, 27, 28], and the $LiTi_{0.05}Mn_{1.95}O_4$ particles exhibit similar characteristic peaks to that of $LiMn_2O_4$ particles. There is no other impurity peak in the XRD patterns of these two samples. These results suggest that the electrolytic MnO_2 completely convert into $LiMn_2O_4$ and a certain amount of titanium ions presents no substantive impact on the spinel structure type of $LiMn_2O_4$ [11]. As for the $LiTi_{0.05}Mn_{1.95}O_4$ octahedrons, the corresponding characteristic diffraction peaks are in almost total agreement with that of $LiTi_{0.05}Mn_{1.95}O_4$ particles and $LiMn_2O_4$ particles, and no other diffraction peaks of manganese oxides and titanium oxides can be observed, which suggests the successful transformation of Mn_3O_4 octahedrons to $LiTi_{0.05}Mn_{1.95}O_4$ sample [2, 26].

Moreover, all the XRD patterns of these three samples does not present the (220) peak, which has much to do with the diffraction of the tetrahedral sites [15, 23]. According to the reported works [29, 30], the doped cations at tetrahedral (8a) sites can cause the emergence of (220) peak even if the amount of doped cation is quite low. Therefore, it can be inferred that the tetravalent titanium ions only replace the tetravalent manganese at octahedral (16d) sites, which can achieve the improvement of structural stability of $LiMn_2O_4$.

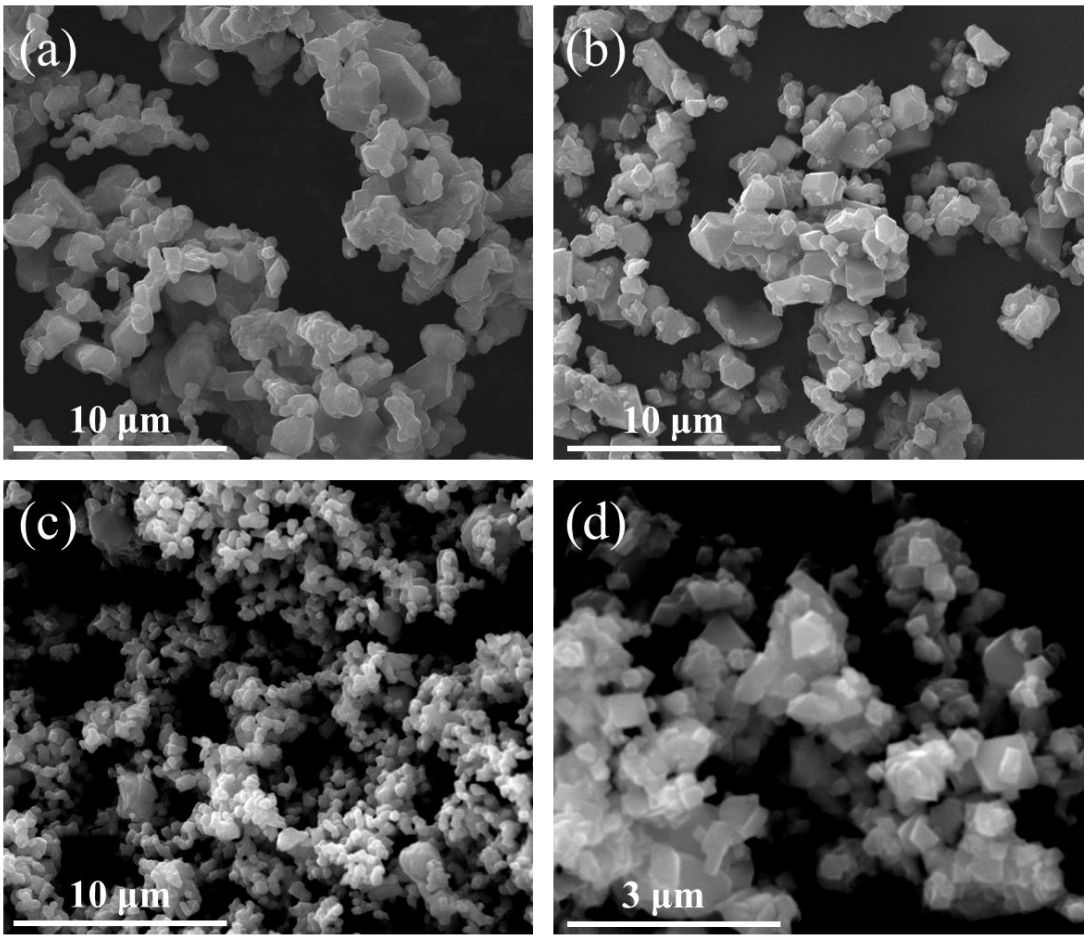

Figure 2. SEM images of $LiMn_2O_4$ particles (a), $LiTi_{0.05}Mn_{1.95}O_4$ particles (b), and $LiTi_{0.05}Mn_{1.95}O_4$ octahedrons (c, d).

Fig. 2 provides the SEM results of $LiTi_{0.05}Mn_{1.95}O_4$ octahedrons, $LiTi_{0.05}Mn_{1.95}O_4$ particles, and $LiMn_2O_4$ particles. The $LiMn_2O_4$ particles (Fig. 2a) present a very unsatisfactory surface morphology with uneven particle size distribution. By contrast, the $LiTi_{0.05}Mn_{1.95}O_4$ particles present relatively uniform particle size distribution. The introduction of titanium ions reduces the particle agglomeration to a great extent. For the $LiTi_{0.05}Mn_{1.95}O_4$ octahedrons shown in Fig. 2c and d, it presents obvious octahedral morphology, which realizes a good inheritance of octahedral morphology of Mn_3O_4 octahedrons. More importantly, this sample also presents uniform particle size distribution, which further contributes to the improvement of electrochemical performance [31-33]. Fig. 3b-e provides the EDS pattern and SEM Mapping images of $LiTi_{0.05}Mn_{1.95}O_4$ octahedrons in the selected area shown in

Fig. 3a, which can present the element composition and distribution. As shown in Fig. 3b, the EDS pattern of $LiTi_{0.05}Mn_{1.95}O_4$ octahedrons possess Mn, O, and Ti elements, which are in agreement with the theoretical design of $LiTi_{0.05}Mn_{1.95}O_4$.

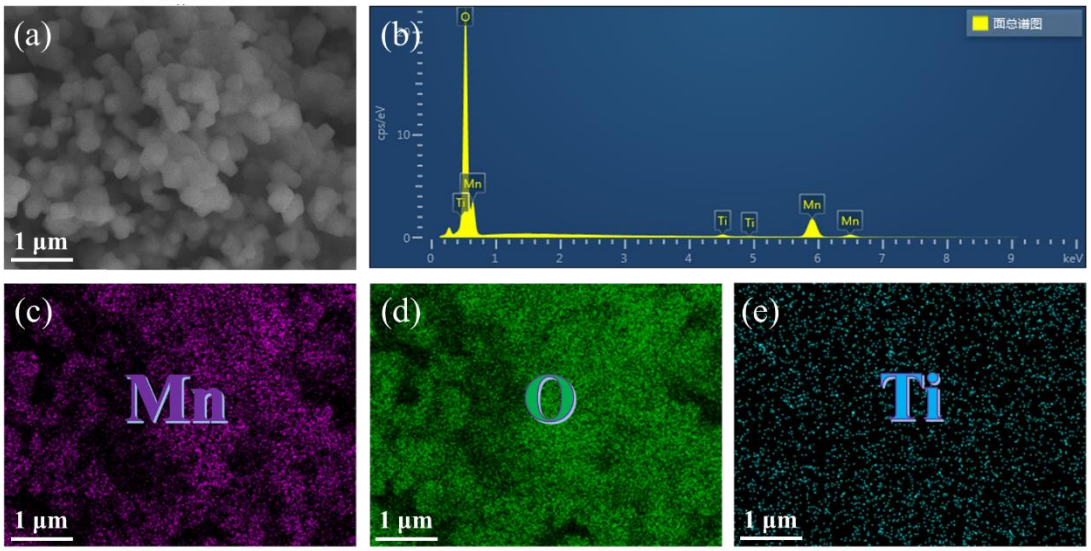

Figure 3. (a) SEM image, (b) EDS pattern, and (c-e) SEM Mapping images of $LiTi_{0.05}Mn_{1.95}O_4$ octahedrons.

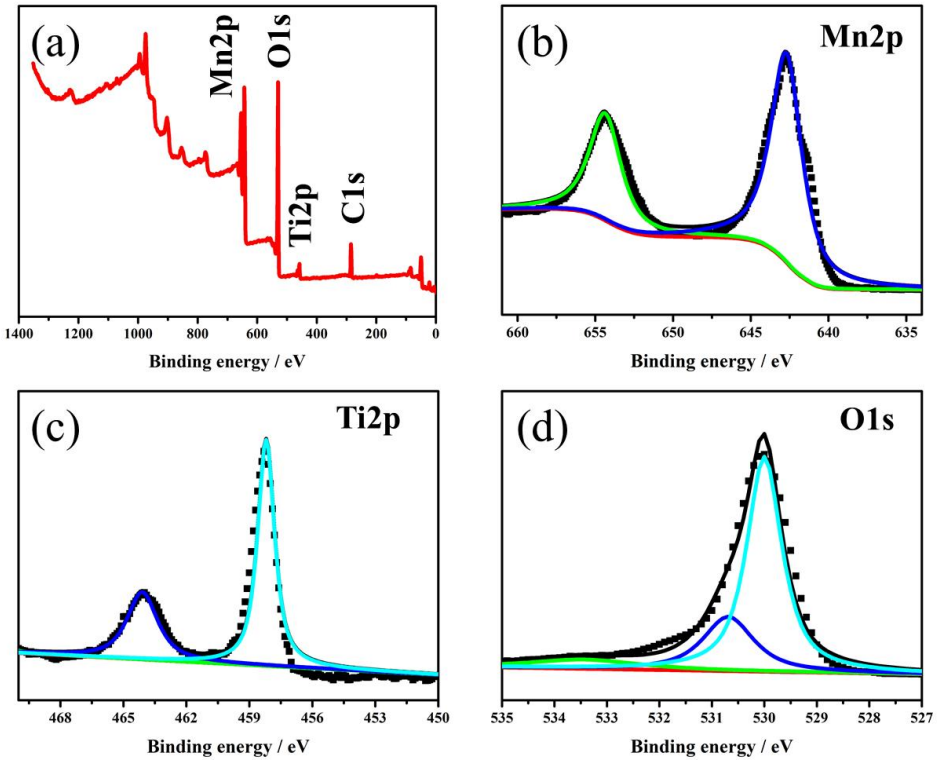

Figure 4. (a) Full XPS spectrum and (b-c) XPS spectra of Mn2p, Ti2p and O1s in $LiTi_{0.05}Mn_{1.95}O_4$ octahedrons.

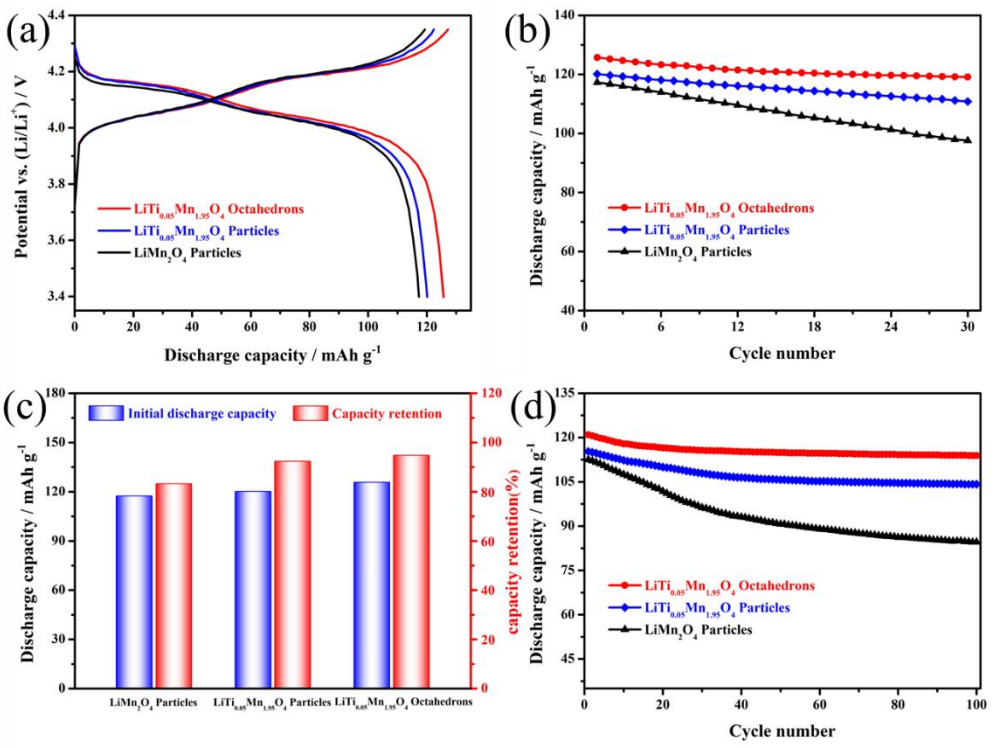

Figure 5. Electrochemical performance of $LiTi_{0.05}Mn_{1.95}O_4$ octahedrons, $LiTi_{0.05}Mn_{1.95}O_4$ particles, and $LiMn_2O_4$ particles: (a) 1st charge-discharge curves, (b) cycling property, (c) histogram comparsion of 1st discharge capacity and capacity retention, and (d) long cycling performance.

The SEM Mapping images (Fig. 3c-e) suggest the uniform distribution of these three elements in $LiTi_{0.05}Mn_{1.95}O_4$ octahedrons. Fig. 4 provides the full XPS spectrum and XPS spectra of Mn2p, Ti2p and O1s in $LiTi_{0.05}Mn_{1.95}O_4$ octahedrons, which can confirm the electronic state of Mn, O, and Ti elements. The full XPS spectrum (Fig. 4a) of $LiTi_{0.05}Mn_{1.95}O_4$ octahedrons presents the existence of Mn2p, O1s, and Ti2p peaks, which are in agreement with the EDS result. Fig. 4b-d provides the XPS spectra of Mn2p, Ti2p and O1s in $LiTi_{0.05}Mn_{1.95}O_4$ octahedrons. As shown here, the binding energy peaks of Mn2p and O1s elements agree with the reported results [29, 31]. The binding energy peaks of Ti2p are divided into Ti 2p3/2 and Ti 2p1/2 at 458.2 and 464.1 eV, suggesting the tetravalent oxidation state of Ti element $LiTi_{0.05}Mn_{1.95}O_4$ octahedrons [20].

The obtained $LiTi_{0.05}Mn_{1.95}O_4$ octahedrons, $LiTi_{0.05}Mn_{1.95}O_4$ particles, and $LiMn_2O_4$ particles were cycled at 0.5 C to investigate the 1st charge-discharge curves (Fig. 5a). All the initial discharge curves of these three samples possesses two obvious voltage platforms, which are in almost total agreement with that of $LiMn_2O_4$. According to the existing literatures [2, 9, 34, 35], these characteristic platforms have strong connections with the lithium intercalation in the process of electrochemical cycling. Fig. 5b exhibits the cycling performance of these three samples at 0.5 C, and Fig. 5c presents the corresponding histogram of 1st discharge capacity and capacity retention. As shown here, the $LiTi_{0.05}Mn_{1.95}O_4$ particles present higher cycling stability than that of the $LiMn_2O_4$ particles, and the $LiTi_{0.05}Mn_{1.95}O_4$ octahedrons presents the optimal electrochemical performance with highest capacity

retention. Such excellent performance is mainly contributed from the synergistic effect between titanium doping and octahedral morphology [2, 20, 24, 26].

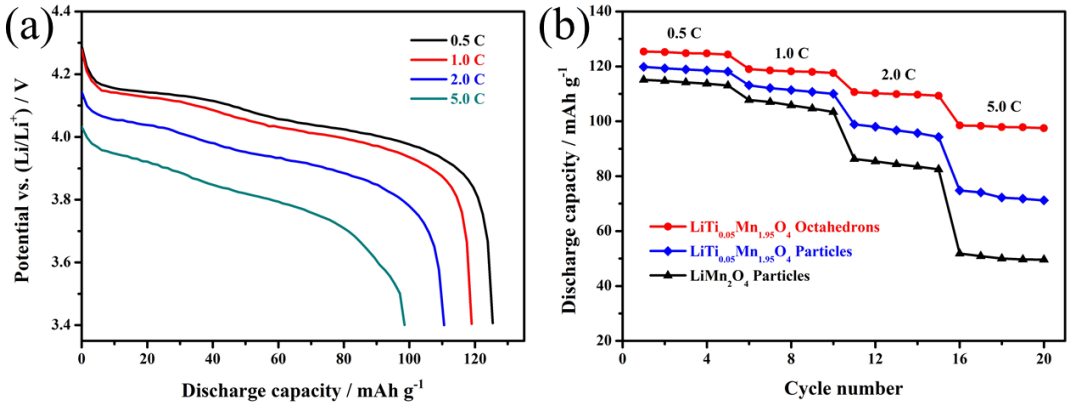

Figure 6. (a) Representative discharge curves of $LiTi_{0.05}Mn_{1.95}O_4$ octahedrons and (b) Rate stability of $LiTi_{0.05}Mn_{1.95}O_4$ octahedrons, $LiTi_{0.05}Mn_{1.95}O_4$ particles, and $LiMn_2O_4$ particles.

Fig. 5d presents the long cycling stability of $LiTi_{0.05}Mn_{1.95}O_4$ octahedrons, $LiTi_{0.05}Mn_{1.95}O_4$ particles, and $LiMn_2O_4$ particles at 1.0 C. It can be seen that the unmodified $LiMn_2O_4$ particles exhibit relatively poor electrochemical performance. The initial reversible capacity only reaches a lower value of 112.5 mAh g^{-1}. After 100 cycles, the discharge specific capacity presents a considerable capacity loss with unsatisfactory capacity retention of 75.2%. For the $LiTi_{0.05}Mn_{1.95}O_4$ particles, the cycling stability was optimized by introducing a certain amount of tetravalent titanium ions. After 100 cycles, the capacity retention of $LiTi_{0.05}Mn_{1.95}O_4$ particles increases to 90.3%. For the undoped $LiMn_2O_4$ sample, the obtained Ti-O chemical bond possesses much higher chemical bond energy than that of the Mn-O chemical bond after introducing a certain amount of tetravalent titanium ions, which efficiently suppresses the two-phase coexistence in the discharge process of $LiMn_2O_4$. Moreover, the introduction of tetravalent titanium ions increases the difference of chemical bonds, which can contribute to reduce the degeneracy of manganese ions to inhibit the Jahn-Teller distortion in the crystal structure [20, 36-38]. As for the $LiTi_{0.05}Mn_{1.95}O_4$ octahedrons, the cycling stability was further optimized by introducing the octahedral morphology. The reversible specific capacity can further increase to 120.9 mAh g^{-1} with excellent capacity retention of 94.2% after 100 cycles. According to the research works [2, 26], the octahedral morphology helped to realize the improvement of cycling stability by inhibiting the manganese dissolution to maintain the structure stability of $LiMn_2O_4$. It is therefore comprehensible that the $LiTi_{0.05}Mn_{1.95}O_4$ octahedrons shows the optimal cyclic stability with excellent capacity retention.

Fig. 6a provides the representative discharge curves of the $LiTi_{0.05}Mn_{1.95}O_4$ octahedrons at different charge-discharge rates. It can be found that the increased cycling rate leads to the gradual vague of voltage platforms. With the increasing of charge-discharge rate, the corresponding voltage platforms in the discharge curves gradually decrease, which has strong connection with the unsatisfactory polarization [39-41]. Fig. 6b provides the corresponding cycling property of $LiTi_{0.05}Mn_{1.95}O_4$

octahedrons, $LiTi_{0.05}Mn_{1.95}O_4$ particles, and $LiMn_2O_4$ particles at different charge-discharge rates. As shown here, the cycling rate has great influence on change of the reversible specific capacity. Especially, the high charge-discharge rate can lead to the serious loss of reversible specific capacity. For the unmodified $LiMn_2O_4$ particles prepared from electrolytic MnO_2, the reversible capacity of 115.1 mAh g^{-1} at 0.5 C has slightly small difference with that of $LiTi_{0.05}Mn_{1.95}O_4$ particles and $LiMn_2O_4$ particles. Unfortunately, the reversible specific capacity rapidly attenuates to 51.8 mAh g^{-1} as the cycling rate reaches up to 5.0 C. By contrast, the $LiTi_{0.05}Mn_{1.95}O_4$ particles present good cycling stability at high charge-discharge rate. The reversible specific capacity of $LiTi_{0.05}Mn_{1.95}O_4$ can increase to 74.8 mAh g^{-1}. Such good performance is closely related to the existence of titanium ions in the spinel crystal structure of $LiTi_{0.05}Mn_{1.95}O_4$ [20, 24]. As for the $LiTi_{0.05}Mn_{1.95}O_4$ octahedrons, the optimal high-rate capability of 98.5 mAh g^{-1} can be achieved at 5.0 C, which has much to do with the further modification of octahedral morphology.

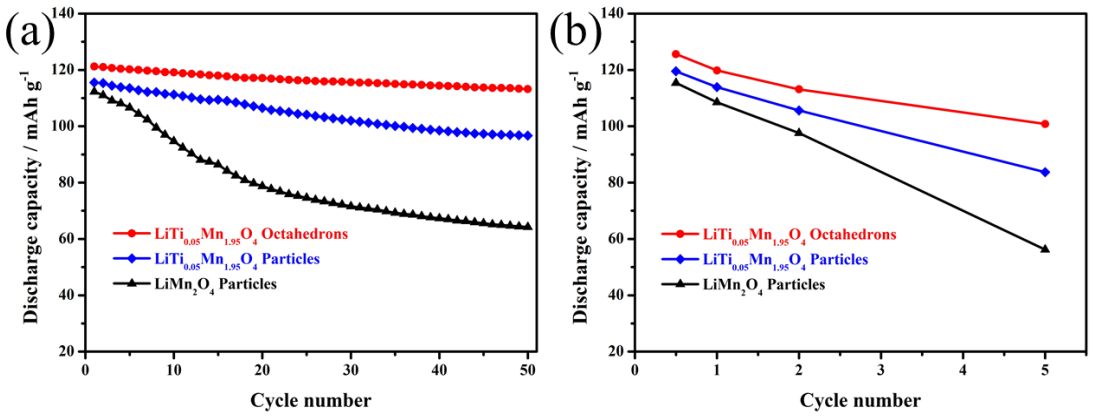

Figure 7. (a) Cycling property and (b) Rate capability of $LiTi_{0.05}Mn_{1.95}O_4$ octahedrons, $LiTi_{0.05}Mn_{1.95}O_4$ particles, and $LiMn_2O_4$ particles at 55 °C.

Fig. 7a presents the cycling performance of $LiTi_{0.05}Mn_{1.95}O_4$ octahedrons, $LiTi_{0.05}Mn_{1.95}O_4$ particles, and $LiMn_2O_4$ particles at 55 °C. The unmodified $LiMn_2O_4$ particles exhibit quite poor elevated-temperature electrochemical performance. The initial discharging specific capacity of 112.3 mAh g^{-1} is similar to the capacity value at room temperature. After 50 cycles, this sample presents a considerable capacity loss with unsatisfactory capacity retention of 57.1%. By contrast, the elevated-temperature cycling stability of $LiTi_{0.05}Mn_{1.95}O_4$ particles (Capacity retention: 83.7%) was optimized by introducing a certain amount of tetravalent titanium ions due to the fact that the Ti-O chemical bond possesses much higher chemical bond energy than that of the Mn-O chemical bond, which has strong connection with the strong crystal structure stability [20, 23, 24]. As for the $LiTi_{0.05}Mn_{1.95}O_4$ octahedrons, the elevated-temperature cycling stability of $LiTi_{0.05}Mn_{1.95}O_4$ sample (Capacity retention: 93.4%) was further optimized by introducing the octahedral morphology. The synergistic interaction of Ti-doping and octahedral morphology significantly enhances the high-temperature electrochemical property of $LiMn_2O_4$. Fig. 7b presents the rate capability of these three samples. It can be found that the

$LiTi_{0.05}Mn_{1.95}O_4$ octahedrons show much better rate performance than that of the $LiMn_2O_4$ particles and $LiTi_{0.05}Mn_{1.95}O_4$ particles. Especially, the $LiTi_{0.05}Mn_{1.95}O_4$ octahedrons shows the optimal rate capability of 100.8 mAh g^{-1} at 5.0 C. However, the $LiMn_2O_4$ particles and $LiTi_{0.05}Mn_{1.95}O_4$ particles only show relatively lower reversible capacity of 83.7 mAh g^{-1} and 56.2 mAh g^{-1}, respectively. For the $LiTi_{0.05}Mn_{1.95}O_4$ octahedrons, the excellent elevated-temperature electrochemical performance has much to do with the synergetic modification of Ti-doping and octahedral morphology [7, 24, 42].

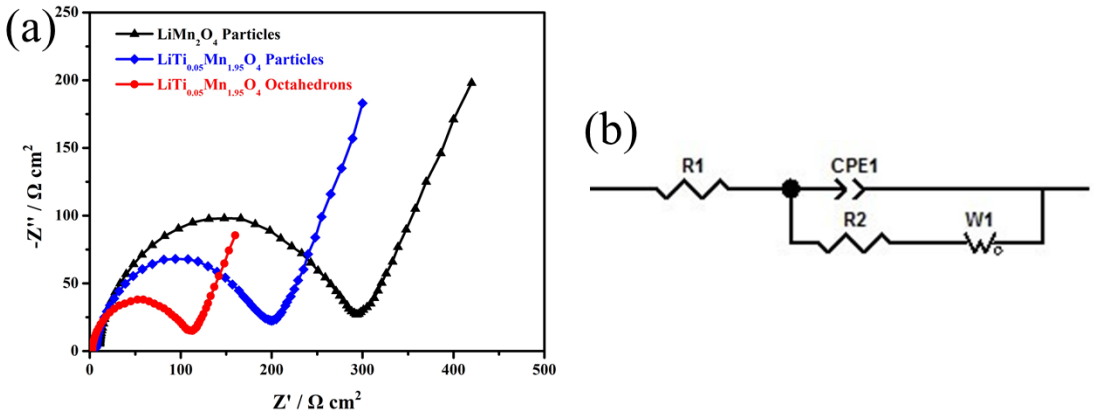

Figure 8. (a) Nyquist plots of $LiTi_{0.05}Mn_{1.95}O_4$ octahedrons, $LiTi_{0.05}Mn_{1.95}O_4$ particles, and $LiMn_2O_4$ particles.

Fig. 8a presents the Nyquist plots of $LiTi_{0.05}Mn_{1.95}O_4$ octahedrons, $LiTi_{0.05}Mn_{1.95}O_4$ particles, and $LiMn_2O_4$ particles, and the corresponding equivalent circuit model is shown in Fig. 8b. According to the reported works [1, 6, 43], the electrochemical performance is closely related to the charge transfer resistance (R_2) in the high-frequency region. Therefore, R_2 values were compared to analyze the electrochemical performance of these three samples. As shown in Fig. 8a, the unmodified $LiMn_2O_4$ particles present relatively large R_2 value (281.3 Ω cm^2), which is in conformance with the poor cycling stability. By contrast, the $LiTi_{0.05}Mn_{1.95}O_4$ particles showed small R_2 value (179.5 Ω cm^2), which has much to do with the introduction of titanium ions in the spinel crystal structure. Especially, the $LiTi_{0.05}Mn_{1.95}O_4$ octahedrons shows the minimum R_2 value (97.2 Ω cm^2), which is mainly contributed by the titanium ions doping and octahedral morphology [20, 24]. Moreover, the uniform particle size distribution is also significant for the improvement of electrochemical property of $LiMn_2O_4$ [29, 31, 32].

4. CONCLUSIONS

To summary, we reported the synthesis of $LiTi_{0.05}Mn_{1.95}O_4$ octahedrons by solid-phase method with Mn_3O_4 octahedrons as manganese precursor and TiO_2 nanoparticles as dopant. The obtained $LiTi_{0.05}Mn_{1.95}O_4$ octahedrons show the characteristic diffraction peaks of $LiMn_2O_4$ without other impure phases. The electrochemical measurements showed that the $LiTi_{0.05}Mn_{1.95}O_4$ octahedrons possess the

optimal cyclic stability compared to the $LiTi_{0.05}Mn_{1.95}O_4$ particles and $LiMn_2O_4$ particles. When cycled at 1.0 C, the $LiTi_{0.05}Mn_{1.95}O_4$ octahedrons presented a relatively satisfactory initial capacity of 120.9 mAh g^{-1}. After 100 cycles, the capacity retention of $LiTi_{0.05}Mn_{1.95}O_4$ octahedrons could reach up to 94.2%, which was much higher than that of other two samples. Moreover, the $LiTi_{0.05}Mn_{1.95}O_4$ octahedrons could exhibit excellent high-rate capability and high-temperature cycling stability. Such excellent performance is mainly contributed from the synergistic effect between Ti-doping and octahedral morphology.

ACKNOWLEDGMENTS
This work was financially supported by the Natural Science Foundation of Henan Province (No. 202300410163), Program for Innovative Research Team (in Science and Technology) in University of Henan Province (No. 20IRTSTHN016), Young Key Teachers Projects in Henan Higher Education Institutions (No. 2018GGJS113), Preferential Scientific Research Projects for Talents Studying Abroad, High-Level Talents Introduction Project of Henan Institute of Science and Technology (No. 203010617011), and University Students' Innovation and Pioneering Project (No. 2021CY002).

References

1. H. Zhao, N. Hu, R. Xu, H. Liu, J. Liu and Q. Ran, *Ceram. Int.,* 46 (2020) 21805.
2. H. Zhao, Y. Nie, Y. Li, T. Wu, E. Zhao, J. Song and S. Komarneni, *Ceram. Int.,* 45 (2019) 17183.
3. H. Liu, M. Li, M. Xiang, J. Guo, H. Bai, W. Bai and X. Liu, *J. Colloid Interface Sci.*, 585 (2021) 729.
4. Q. Liu, Q. Liang, J. Guo, M. Xiang, W. Bai, H. Bai and X. Liu, *Ceram. Int.,* 47 (2021) 2441.
5. R. Chen, B. Wen, H. Li, M. Xiang, C. Su, J. Guo, W. Bai and Z. Sa, *Vacuum,* 187 (2021) 110077.
6. J. Zhu, Q. Liu, M. Xiang, J. Guo, H. Bai, X. Liu, C. Su and W. Bai, *Ceram. Int.,* 46 (2020) 14516.
7. S. Wang, H. Liu, M. Xiang, J. Guo, W. Bai, H. Bai, X. Liu and C. Su, *New J. Chem.*, 44 (2020) 10569.
8. J. Cao, S. Guo, R. Yan, C. Zhang, J. Guo and P. Zheng, *J. Alloy. Compd.,* 741 (2018) 1.
9. J. Liu, G. Li, H. Bai, M. Shao, C. Su, J. Guo, X. Liu and W. Bai, *Solid State Ionics*, 307 (2017) 79.
10. X. Yu, J. Deng, X. Yang, J. Li, Z.-H. Huang, B. Li and F. Kang, *Nano Energy.* 67 (2020) 104256.
11. J. Abou-Rjeily, I. Bezza, N.A. Laziz, C. Autret-Lambert, M.T. Sougrati and F. Ghamouss, *Energy Storage Mater.,* 26 (2020) 423.
12. J.T. Son and H.G. Kim, *J. Power Sources*, 147 (2005) 220.
13. D.-W. Han, W.-H. Ryu, W.-K. Kim, J.-Y. Eom and H.-S. Kwon, *J. Phys. Chem. C*, 117 (2013) 4913.
14. M.-Y. Zhao, Z.-Y. Ji, Y.-G. Zhang, Z.-Y. Guo, Y.-Y. Zhao, J. Liu and J.-S. Yuan, *Electrochim. Acta*, 252 (2017) 350.
15. H. Zhao, F. Li, X. Liu, C. Cheng, Z. Zhang, Y. Wu, W. Xiong and B. Chen, *Electrochim. Acta*, 151 (2015) 263.
16. Y. Fu, H. Jiang, Y. Hu, Y. Dai, L. Zhang and C. Li, *Ind. Eng. Chem. Res.,* 54 (2015) 3800.
17. H. Zhao, X. Bai, J. Wang, D. Li, B. Li, Y. Wang, L. Dong, B. Liu and S. Komarneni, *Materials.* 11 (2018) 1558.
18. Guo Shaohua, Zhang Shichao, He Xiangming, Pu Weihua, Jiang Changyin and W. Chunrong, *J. Electrochem. Soc.*, 155 (2008) A760.
19. H. Zhao, D. Li, Y. Wang, F. Li, G. Wang, T. Wu, Z. Wang, Y. Li and J. Su, *Materials*, 11 (2018) 1455.

20. L. Xiong, Y. Xu, C. Zhang, Z. Zhang and J. Li, *J. Solid State Electr.*, 15 (2010) 1263.
21. N. Jayaprakash, N. Kalaiselvi, Gangulibabu and D. Bhuvaneswari, *J. Solid State Electr.*, 15 (2010) 1243.
22. A. Iturrondobeitia, A. Goñi, V. Palomares, I. Gil de Muro, L. Lezama and T. Rojo, *J. Power Sources*, 216 (2012) 482.
23. L. Xiong, Y. Xu, T. Tao and J.B. Goodenough, *J. Power Sources*, 199 (2012) 214.
24. Xue Jing, Zhang Hu, Yang Tuoying and Z. Xiuxing, *Int. J. Electrochem. Sc.*, (2020) 8732.
25. Y. Cai, Y. Huang, X. Wang, D. Jia, W. Pang, Z. Guo, Y. Du and X. Tang, *J. Power Sources*, 278 (2015) 574.
26. G. Jin, H. Qiao, H. Xie, H. Wang, K. He, P. Liu, J. Chen, Y. Tang, S. Liu and C. Huang, *Electrochim. Acta*, 150 (2014) 1.
27. H. Zhao, S. Liu, Z. Wang, Y. Cai, M. Tan and X. Liu, *Electrochim. Acta*, 199 (2016) 18.
28. Y. Jin, S. Wang, J. Li, S. Qu, L. Yang and J. Guo, *RSC Adv.*, 10 (2020) 22848.
29. H. Zhao, X. Liu, C. Cheng, Q. Li, Z. Zhang, Y. Wu, B. Chen and W. Xiong, *J. Power Sources*, 282 (2015) 118.
30. X. Yi, X. Wang, B. Ju, Q. Wei, X. Yang, G. Zou, H. Shu and L. Hu, *J. Alloy. Compd.*, 604 (2014) 50.
31. H. Zhao, S. Liu, Y. Cai, Z. Wang, M. Tan and X. Liu, *J. Alloy. Compd.*, 671 (2016) 304.
32. H. Zhao, S. Liu, Z. Wang, Y. Cai, M. Tan and X. Liu, *Ceram. Int.*, 42 (2016) 13442.
33. Z. Wang, J. Du, Z. Li and Z. Wu, *Ceram. Int.*, 40 (2014) 3527.
34. H. Zhao, F. Li, X. Liu, W. Xiong, B. Chen, H. Shao, D. Que, Z. Zhang and Y. Wu, *Electrochim. Acta*, 166 (2015) 124.
35. H. Zhao, Y. Li, D. Shen, Q. Yin and Q. Ran, *J. Mater. Res. Technol.*, 9 (2020) 7027.
36. L.-X. Zhang, Y.-Z. Wang, H.-F. Jiu, Y.-L. Wang, Y.-X. Sun and Z. Li, *Electron. Mater. Lett.*, 10 (2014) 439.
37. L. Xiao, Y. Zhao, Y. Yang, Y. Cao, X. Ai and H. Yang, *Electrochim. Acta*, 54 (2008) 545.
38. G.-M. Song, W.-J. Li and Y. Zhou, *Mater. Chem. Phys.*, 87 (2004) 162.
39. L. Liang, M. Xiang, W. Bai, J. Guo, C. Su, L. Yang, H. Bai and X. Liu, *J. Mater. Sci-Mater. El.*, 31 (2019) 286.
40. Y. Yu, M. Xiang, J. Guo, C. Su, X. Liu, H. Bai, W. Bai and K. Duan, *J. Colloid Interface Sci.*, 555 (2019) 64.
41. S. Wang, M. Xiang, Y. Lu, J. Guo, C. Su, H. Bai and X. Liu, *J. Mater. Sci-Mater. El.*, 31 (2020) 6036.
42. H. Zhao, X. Gao, Y. Li, Q. Ran, C. Fu, Y. Feng, J. Liu, X. Liu and J. Su, *Ceram. Int.*, 45 (2019) 17591.
43. H. Zhang, Y. Xu, D. Liu, X. Zhang and C. Zhao, *Electrochim. Acta*, 125 (2014) 225.